Title:

Automation and optimization of in-situ assessment of wall thermal transmittance using a Random Forest algorithm

Authors:

David Bienvenido-Huertas[1], Carlos Rubio-Bellido*[2], Juan Luis Pérez-Ordóñez[3], Miguel José Oliveira[4]

[1]Department of Graphical Expression and Building Engineering, University of Seville, 41012 Seville, Spain; jbienvenido@us.es
[2]Department of Building Construction II, University of Seville, 41012 Seville, Spain; carlosrubio@us.es
[3]Department of Civil Engineering, University of A Coruña, E.T.S.I. Caminos, Canales y Puertos, 15071 A Coruña, Spain; jlperez@udc.es
[4]Instituto Superior de Engenharia, Universidade do Algarve, 8005-139 Faro, Portugal; mjolivei@ualg.pt

*Author to whom correspondence should be addressed;
Higher Technical School of Building Engineering, Ave. Reina Mercedes 4A, Seville, Spain
E-Mail: carlosrubio@us.es (C.R.B.); Tel.: +34-686-135-595

Highlights:

Artificial intelligence applied to thermal characterization of façades.
Random Forest algorithms designed for heat flow meter method and thermometric method.
Suitability of Random Forest to apply ISO 6946.
Accurate determination of the building period of a wall.

Abstract:

Reducing energy consumption and greenhouse gases emissions is among the main challenges of building sector. It is therefore crucial to know the characteristics of envelopes. There are experimental methods to determine thermal transmittance, but limitations are presented. By using techniques of artificial intelligence, this article solves the limitations of current methods by predicting correctly the thermal transmittance value of ISO 6946 and the building period of a wall with monitored data. The methodology used is extrapolated to any country: 163 real monitorings and 140 different typologies of walls have been combined to generate the dataset (22,820 items). The results show the optimal operation of the Random Forest algorithm because both the thermal transmittance of ISO 6946 and the building period are determined by using the most common methods: the heat flow meter method and the thermometric method. This study makes progress towards more automatized processes to characterize thermal transmittance.

Keywords:

Thermal transmittance; ISO 6946; building period; Random Forests; artificial intelligence; in-situ

Nomenclature	
Symbols	
a_i	Actual U_{6946} [W/(m²K)]
e_i	Estimated U_{6946} [W/(m²K)]
F	Distribution of negative samples
F_{EXT}	External total thermal mass factor obtained from the external thermal mass factor of each layer [J/(m²·K)]
F_{INT}	Total internal thermal mass factor obtained from the internal thermal mass factor of each layer [J/(m²·K)]
G	Distribution of positive samples
h	Heat transfer coefficient [W/(m²K)]
h_{in}	Total internal heat transfer coefficient [W/(m²K)]
n	Number of observations in the dataset
p_e	Hypothetical probability of agreement by chance
p_o	Relative observed agreement among the observers
Q	Thermal energy [J]
q_j	Density of the heat flow rate per unit area [W/m²]

R^2	Coefficient of determination
$R_{s,ext}$	External surface thermal resistance [(m²·K)/W]
$R_{s,int}$	Internal surface thermal resistance [(m²·K)/W]
S	Heat transfer surface area of the body [m²]
s_i	Thickness of each wall layer [m]
T	Body temperature [K]
$T_{environment}$	Environment temperature [K]
$T_{int,j}$	Internal air temperature [K]
$T_{ext,j}$	External air temperature [K]
$T_{s,int,j}$	Internal surface temperature of the wall [K]
U_{6946}	Thermal transmittance obtained by ISO 6946 [W/(m²K)]
U_{HFM}	Thermal transmittance obtained by the average method of ISO 9869−1 [W/(m²K)]
$U_{HFM-storage}$	Thermal transmittance obtained by the average method with correction for storage effects of ISO 9869−1 [W/(m²K)]
$U_{in-situ}$	Thermal transmittance value obtained by some of the experimental procedures [W/(m²K)]
U_{THM}	Thermal transmittance obtained by the thermometric method [W/(m²K)]

Greek letters

Δt	Time interval between both readings [s]
δT_{EXT}	Difference between the average external air temperature in the 24 h before measuring the observation and the average external air temperature in the first 24 h of the test [K]
δT_{INT}	Difference between the average internal air temperature in the 24 h before measuring the observation and the average internal air temperature in the first 24 h of the test [K]
λ_i	Thermal conductivity of each wall layer [W/(m·K)]

Abbreviations

BFGS	Broyden-Fletcher-Goldfarb-Shanno
CART	Classification and Regression Tree
FP	False positive
HFM	Heat flow meter method
MAE	Mean absolute error
MLP	Multilayer perceptron

1. Introduction

The decrease of building energy consumption is one of the main challenges of today's society. In the 2015 Paris Climate Conference, 195 countries committed to significantly reducing greenhouse gas emissions. The building sector has a key role as it is responsible for a high percentage of energy consumption and greenhouse gas emissions [1], so bodies and institutions have established ambitious goals to improve the energy performance of buildings. Regarding the European Union, its roadmap towards a low-carbon economy aims at decreasing emissions by 90% with respect to the levels of 1990 [2].

Consequently, reducing building energy consumption is crucial to achieve such goal. Most consumption is caused by using HVAC systems [3,4], so it is essential to know the thermal performance of building envelopes to accurately know their energy requirement and establish energy conservation measures [5,6]. In recent years, many studies have been focused on the thermal characterization of envelopes, namely the experimental characterization of thermal transmittance [7].

The thermal transmittance (also known as U-value) of walls can be experimentally characterized by various procedures. The most used are the heat flow meter method (HFM) and the thermometric method (THM) (also known as "Air-Surface Temperature Ratio Method") (see Figure 1) [7]. HFM is developed in ISO 9869-1 [8] through various procedures, with the average procedure being the most used [7]. This procedure considers that the average of instantaneous values of heat flux and internal-external temperature differences reduce oscillations and lead to a steady state:

$$U_{HFM} = \frac{\sum_{j=1}^{n} q_j}{\sum_{j=1}^{n} (T_{int,j} - T_{ext,j})} \tag{1}$$

where q_j [W/m²] is the density of the heat flow rate per unit area, and $T_{int,j}$ and $T_{ext,j}$ [K] are the internal and external air temperatures. The method therefore operates by measuring both the heat flux and the internal and external air temperature. Some studies show the limitations and requirements to be considered when monitoring walls. Cesaratto et al. [9], Desogus et al. [10], and Trethowen [11] found that one of the main error contributions in the method was due to the heat flux measurement. Meng et al. [12] established that the error associated with placing the heat flux plate can be up to 26%. Also, the need to guarantee a high thermal gradient [10,13], the orientation of the wall [14], and no condensations

[15] nor freezes [16] in the wall have been reflected in several studies to ensure representative results [10,13]. Finally, the minimum duration of tests depends on the wall thermal transmittance and the variability of environmental conditions [17], achieving durations between 3 and 7 days [7,18].

Due to the variability of performance presented by HFM, many research studies have analysed the application of the method in a great variety of case studies and the adjustment degree of results: (i) Ficco et al. [19] studied the adjustment degree of HFM in 6 walls of various materials by using 3 different plates, and low deviation was obtained in tests. HFM therefore obtained representative results despite the possible limitations associated with the method because of using the heat flux plate and because of environmental aspects; (ii) Evangelisti et al. [20] used HFM to assess a wall with a balcony and a wall with a portico. The heat transfer coefficients obtained with HFM were compared with other different expressions obtained both from experimental correlations and ISO 6946. The results reflected disparity in the convective correlations in comparison with the values obtained by HFM; (iii) a similar study was conducted by Asdrubali et al. [21], who analysed 6 eco-efficient walls. The adjustment degree of results oscillated between 4 and 75%. The authors considered that the variability of the environmental conditions during the test and the overestimation of the thermal conductivity values were the possible reasons of the percentage deviations; (iv) Gaspar et al. [13] studied the performance of HFM in a wall with low thermal transmittance. The authors determined that keeping a temperature difference of 19ºC between the interior and the exterior reduced the test duration up to 72 h, with an appropriate adjustment degree. If the test is performed with a lower thermal gradient, then the test duration will be increased; (v) Lucchi [22,23] assessed historical brick and stone walls in Italy with HFM. There were deviations between the measured values and the values tabulated and calculated according to the Italian energy regulation for buildings; and (vi) these deviations between tabulated procedures and HFM were also reflected by Rotilio et al. [24], who monitored 4 historic walls in Fontecchio (Italy). The results reflected deviations of up to 15% between the value obtained by HFM and the value established by the Italian regulation.
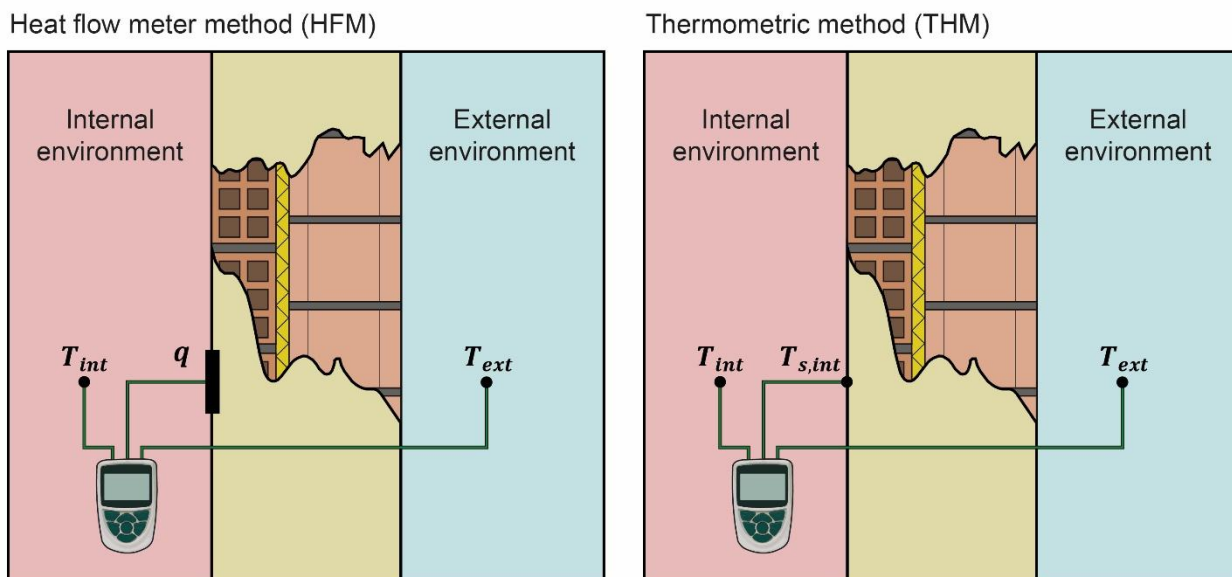

Figure 1. Schemes of the heat flow meter method and the thermometric method.

As there are both difficulties in performing HFM and possible errors associated with environmental and morphological factors of walls, the infrared thermography has emerged in recent years as an alternative for HFM. These approaches aimed at measuring the surface temperature of walls and determining variables of radiation transfer, such as the emissivity or the reflected apparent temperature [25]. The main difference between methods is due to the location of the chamber during the test and the formulation used. Methods from the exterior [26,27] and from the interior [28–30] can therefore be distinguished. The main advantage of these methods is that, if the thermal gradient is high and test are conducted with low wind speeds and without rainfalls, then the thermal characterization can be made in a short space of time [26]. Also, the thermal heterogeneities presented by the wall can be evaluated by using an infrared camera [30]. However, the many possibilities of formulation have implied a great variety of approaches. Bienvenido-Huertas et al. [31,32] analysed the different possibilities of formulation of the internal and external methods. The results reflected an acceptable adjustment degree of correlations of dimensionless numbers with HFM. This fact is in accordance with the last research studies conducted by Tejedor et al. [30,33] related to the thermography method.

THM is another alternative of HFM. THM is a method in which the heat flux measurement is replaced with the surface temperature measurement [34,35] because of the error sources associated with the heat flux in the determination of thermal transmittance [11,12]. THM is based on the Newton's Law of Cooling, which establishes that, when the temperature difference between a body and the environment is not considerable, the rate of heat transfer by conduction, convection, and radiation is almost proportional to the temperature difference between the body and the environment:

$$\frac{dQ}{dt} = S \cdot h \cdot [T - T_{environment}] \tag{2}$$

where Q [J] is the thermal energy, S [m^2] is the heat transfer surface area of the body, h [W/(m^{2}K)] is the heat transfer coefficient, T [K] is the body temperature, and $T_{environment}$ [K] is the environment temperature. Through Eq. (2), the heat flux can be expressed with a new expression (Eq. (3)). By using Eq. (3), Eq. (1) can be modified, thus obtaining the expression used for THM (Eq. (4)).

$$q_j = h_{in}\left(T_{int,j} - T_{s,int,j}\right) \tag{3}$$

$$U_{THM} = \frac{\sum_{j=1}^{n} h_{in}\left(T_{int,j} - T_{s,int,j}\right)}{\sum_{j=1}^{n}\left(T_{int,j} - T_{ext,j}\right)} \tag{4}$$

where h_{in} [W/(m^{2}K)] is the total internal heat transfer coefficient, and $T_{s,int,j}$ [K] is the surface temperature of the wall from the interior. THM has been used in several studies, thus showing the possibility of being used to determine the thermal transmittance of walls. Kim et al. [36] used both THM and HFM in 4 different walls before and after improvement performances. The average error in the 8 tests between THM and HFM was 3.21%. Later, Kim et al. [35]analysed 4 different case studies by studying walls with different orientations. The error analysis was lower than 10% between HFM and THM. There are, however, limitations in relation to the use of the method due to the value or expression used for the total internal heat transfer coefficient [7]. The use of theoretical values for total heat transfer coefficients can lead to important deviations [32]. The correct use of the method in typical walls and under acceptable conditions therefore ensures representative results to be obtained [32,36].

A common practice to guarantee representative experimental results is using the criterion included in Section 7.3 from ISO 9869-1 [7], which indicates that the percentage deviation between the measured value and the thermal transmittance value of ISO 6946 [37] should not be greater than 20% (see Eq. (5)). If there is higher deviation, there can be an error in monitorings. This validation procedure has been widely used in many studies focused on the validation of experimental methods, including HFM [38], THM [34] , and the quantitative infrared thermography [30], among others. However, its use has some limitations due to the calculation procedure of ISO 6946 [37], which is carried out by considering the wall as an element of parallel layers, and each layer with a thermal resistance. The thermal transmittance is obtained by the inverse of the sum of the thermal resistances of layers (which are obtained through the thermal conductivity and the thickness of each) and surface thermal resistances (see Eq. (6)).

$$\alpha = \frac{U_{in-situ} - U_{6946}}{U_{6946}} \tag{5}$$

$$U_{6946} = \frac{1}{R_{s,int} + \sum_{i=1}^{n} \frac{s_i}{\lambda_i} + R_{s,ext}} \tag{6}$$

where $U_{in-situ}$ [W/(m^{2}K)] is the thermal transmittance value obtained by some of the experimental procedures, U_{6946} [W/(m^{2}K)] is the thermal transmittance value of ISO 6946, λ_i [W/(m·K)] and s_i [m] are the thermal conductivity and the thickness of each wall layer, respectively, and $R_{s,int}$ and $R_{s,ext}$ [(m^2·K)/W] are the internal and external surface resistances, respectively.

The number, type, and characteristics of the layers of walls are needed for the calculation procedure included in ISO 6946, so the main limitation is related to the determination of the wall configuration [19]. The wall configuration can be determined by various procedures: (i) endoscopic analysis [19,39], (ii) use of technical documents of the building [40], and (iii) estimations based on analogous buildings [19,40]. Among these three techniques, estimations based on analogous buildings have the highest uncertainty [19,21], so the endoscopy and the use of technical documents are the most efficient [19]. Although the endoscopic analysis and estimations based on analogous buildings carry out more accurate calculations, both the lack of technical documents on the characteristics of the envelope and the damages generated by endoscopic techniques limit the correct use of ISO 6946 [7]. Also, the possible variation of the thermal conductivity of layers (generally obtained through technical catalogues [7]) increases the error in the estimation of thermal transmittance.

The ISO 9869-1 standard includes a different procedure to carry out corrections for the heat storage effect [8]. This new procedure consists in modifying the heat flux through a correction obtained for the heat storage of the materials of the wall (see Eq. (7)). More detailed information on this calculation methodology can be found in [7].

$$U_{HFM-storage} = \frac{\sum_{j=1}^{n} q_j - \frac{(F_{INT}\delta T_{INT} + F_{EXT}\delta T_{EXT})}{\Delta t}}{\sum_{j=1}^{n}\left(T_{INT,j} - T_{EXT,j}\right)} \tag{7}$$

where F_{INT} [J/(m^2·K)] is the total internal thermal mass factor obtained from the internal thermal mass factor of each layer, δT_{INT} [K] is the difference between the average internal air temperature in the 24 h before measuring the observation and the average internal air temperature in the first 24 h of the test, F_{EXT} [J/(m^2·K)] is the external total thermal mass factor obtained from the external thermal mass factor of each layer, δT_{EXT} [K] is the difference between the average external air temperature in the 24 h before measuring the observation and the average external air temperature in the first 24 h of the test, and Δt [s] is the time interval between both readings. To use this new procedure is therefore

important to know the thermophysical properties of the materials of the wall similarly as in ISO 6946. As a result, the procedure has the same use limitations as the method of ISO 6946. Some studies, however, stress the potential of using the procedure of heat storage effect: (i) Choi and Ko [41] found that the use of the correction procedure reduced the duration required for tests. In this way, the method with correction achieved a standard deviation of 0,036 two days later, and of 0,006 four days later, whereas the average method obtained a deviation of 0,160 five days later, thereby concluding that the use of the correction procedure reduced the time required for monitoring; and (ii) Deconinck et al. [42] drew a similar conclusion: for the average method, a period of 8 days was required to obtain a low deviation in the results, whereas the time required for the correction procedure was 3 days. So, the limitations of the procedure related to the determination of thermophysical properties should be solved. In a recent study, Bienvenido-Huertas et al. [43] analysed the use of multilayer perceptrons (MLPs) to carry out the correction procedure without knowing the thermophysical properties of a wall. Different input variables, some of them from the monitoring of a wall (e.g., the internal air temperature), were considered. However, new variables were included, such as the thickness of the wall and the building period in which it was designed and built. The results achieved an acceptable adjustment degree between the value estimated by the MLP and the actual value obtained by knowing the thermophysical properties of a wall. Although the building period can be determined with cadastral data of buildings, there can be some limitations for its correct classification, particularly in buildings designed and built in the transition years of the periods or in buildings from old periods which have been renovated (consulting the cadastral data of the building would indicate the year of construction and not the year of improvement). Later, the same input variables were used to determine the results of ISO 9869-1 with THM [44], as there could be possible deviations between the results of both methods because of the total internal heat transfer coefficient used in THM [32,45]. The MLPs made accurate estimations of the thermal transmittance values of ISO 9869-1, thus reducing the possible deviations between both methods.

2. Aims of this research

Limitations in thermal transmittance assessments were found in previous reviews, namely (i) the determination of thermal transmittance through ISO 6946 to evaluate the percentage deviation of experimental results according to the criterion included in Section 7.3 from ISO 9869-1; and (ii) the determination of building periods to use optimization approaches based on MLPs. This study therefore aims at tackling such weaknesses in in-situ assessments. The objective was to accurately determine both variables, thus automating and optimizing the data analysis. For this purpose, the use of artificial intelligence is an opportunity to optimize and automate certain processes. Moreover, creating datasets with a high number of cases through simulations is an opportunity to generate artificial intelligence models due to the adjustment degree between the simulated and actual values under certain boundary conditions [46,47]. Random Forest was used in this study as an algorithm of artificial intelligence. It is widely validated and used in various applications of building energy analysis [48–50] and also tackles classification and regression problems. Another new aspect of this study is the lack of studies using Random Forests for problems related to the thermal characterization of building envelopes.

This article is structured as follows: after the introduction, Section 3 describes how the Random Forest algorithm operates. Section 4 describes the methodology: the variables used in the different approaches, the dataset designed, and the training and validation of models. Section 5 discusses the results obtained. Finally, Section 6 includes the main conclusions.

3. Random Forest algorithm

Tree-type algorithms are among the algorithms of artificial intelligence applied to classification and regression problems. The most known is the Classification and Regression Tree (CART) algorithm [51], which constructs prediction models with a reverse tree structure (i.e., from the root to the leaves, with the root being in the upper part of the model's scheme). Prediction models are suitable for classification and regression problems (i.e., the output can be a label or a numeric value). The structure of the tree is made up of internal nodes corresponding to each variable considered for predicting the model, arches corresponding to the value or range of values of the variable, and leaves corresponding to the output value of the model.

Although the CART model has been widely used in many applications [52,53], several studies show limitations of its use [54,55]. The Random Forest (RF) algorithm is therefore an opportunity to use tree models with a better performance. RF operates by creating a set of CART models based on the training subset so that a forest of tree models is generated (see Figure 2). As it is an ensemble learning algorithm, a better performance than CART is obtained [56] and the variance and bias of the model are reduced [57,58]. Moreover, RF develops efficient models with big dataset and is not influenced by atypical values [59]. The number of trees considered in the algorithm strongly affect the performance of the RF model [60].
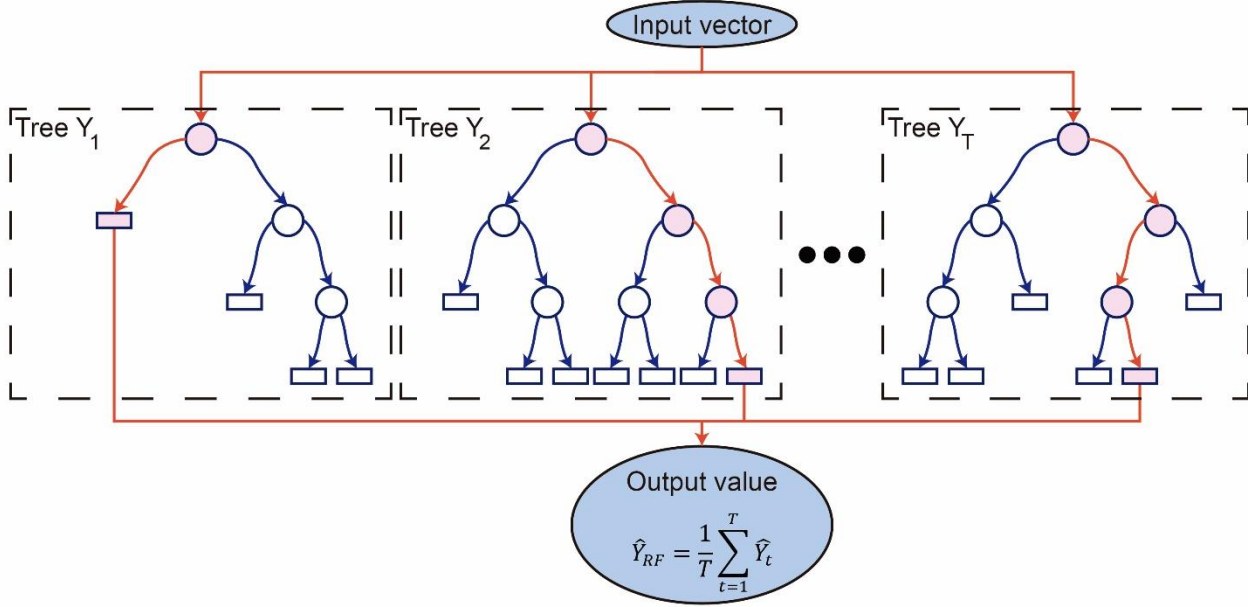
Figure 2. Scheme of the operation of a Random Forest model.

For training an RF model, the training subset is divided into N bootstrapped sample sets [58], and each bootstrapped sample generates a CART model. Also, each node of each CART is divided by using a subset of m predictors randomly selected, thus reducing the influence of the strongest predictors [61]. The estimation given by the RF model is obtained by the average of the estimations given by the set of CART models:

$$\hat{Y}_{RF} = \frac{1}{T} \sum_{t=1}^{T} \hat{Y}_t \tag{8}$$

where $\hat{Y}_t$ is the output of the t-th tree and T is the number of trees.

4. Methodology

4.1. Approaches

As noted earlier, this study aims at solving two main problems: the determination of the thermal transmittance value of ISO 6946 and the building period of the wall analysed. For this purpose, monitored data were used. It is therefore important to make distinctions between the approaches according to the type of the output variable intended to be estimated by the model. Also, independent models were developed according to the experimental procedure used to assess the thermal transmittance: HFM or THM. Table 1 includes the input and output variables for each approach, as well as their nomenclature. Input variables have always the same structure in the different approaches: the maximum and minimum value recorded by each variable in the tests are used, as well as the average value obtained by the instantaneous measurements throughout the whole test. This was performed both for the internal and external air temperature. The difference related to the in-situ method used in the monitoring (HFM or THM) is the third variable monitored: in HFM, the heat flux, and in THM, the internal surface temperature of the wall. In THM, the coefficient of internal heat transfer is not considered as an input variable because the approaches used in the scientific literature do not need additional variables to quantify it: either using a theoretical value for the coefficient of the total heat transfer [34] or experimental correlations characterizing it through the surface temperature [32]. The other two variables considered were the thickness of the wall and the test time. The output variable was a numeric type (U_{6946}) or a label (building period) depending on the approach. As the scope of this study was Spain, the response given by the model for the building period was 3 different periods: P1 (anterior to the normative NBE-CT-79 [62]), P2 (posterior to NBE-CT-79 and anterior to the Spanish Technical Building Code [63]), and P3 (posterior to the Spanish Technical Building Code).

Table 1. Input and output variables used in each approach.

Approach	In-situ method	Input variables	Output variables
Thermal transmittance of ISO 6946	HFM	$\bar{T}_{int}$, max (T_{int}), min (T_{int}), $\bar{T}_{ext}$, max (T_{ext}), min (T_{ext}), $\bar{q}$, max (q), min (q), thickness, time	U_{6946}
	THM	$\bar{T}_{int}$, max (T_{int}), min (T_{int}), $\bar{T}_{ext}$, max (T_{ext}), min (T_{ext}), $\bar{T}_{s,int}$, max $(T_{s,int})$, min $(T_{s,int})$, thickness, time	U_{6946}
Building period	HFM	$\bar{T}_{int}$, max (T_{int}), min (T_{int}), $\bar{T}_{ext}$, max (T_{ext}), min (T_{ext}), $\bar{q}$, max (q), min (q), thickness, time	Building period (P1, P2, and P3)

THM	$\bar{T}_{int}$, max (T_{int}), min (T_{int}), $\bar{T}_{ext}$, max (T_{ext}), min (T_{ext}), $\bar{T}_{s,int}$, max $(T_{s,int})$, min $(T_{s,int})$, thickness, time	Building period (P1, P2, and P3)

4.2. Dataset used

To obtain representative results of the application of RF models, many tests were required. Performing many tests implies a temporary effort and the limitation of applying the models in other regions (e.g., as tests should be adapted to the building periods or type of walls of each zone), so transient two-dimensional simulations were conducted with finite element methods. A total of 163 real monitorings were first carried out in various walls, both under favourable conditions to apply experimental methods (i.e., with a high thermal gradient) and unfavourable conditions. It is important to note that the duration was different, ranging from 3 to 7 days. The monitorings were useful to have 163 sets of time series of the internal and external air temperature. Afterwards, 140 typologies of different walls in the building stock in Spain were designed. By using various sources, such as [64–66], accurate knowledge of the design used in the façades of the building stock in Spain was obtained (i.e., accurate knowledge of the number of layers, type of material, thermal conductivities, and thicknesses of a representative sample of the Spanish building stock was available). The error associated with the determination of thermal transmittance was therefore reduced, as many studies indicate (by using accurate thermal transmittance values as output variables, without errors due to the lack of knowledge of materials or thermal properties of walls). The walls designed were of different typologies according to the building period, existing typologies with or without insulating material, and with or without air gaps. The different 140 typologies of walls were useful to design the 2D models. The 163 sets of time series were used as boundary conditions. By combining 140 wall typologies with 163 monitorings, a total of 22,820 different combinations were obtained. A transient two-dimensional simulation was performed in each combination with data of internal and external air temperature, thereby obtaining the variables of the internal surface temperature and the heat flux required for using HFM and THM. The values established in ISO 6946 were selected as surface thermal resistances of boundary conditions: 0.04 m²K/W for external conditions and 0.13 m²K/W for internal conditions. The standard recommends these values for the typical building envelopes [37]. These values have also been used in other similar research studies on thermal characterization through transient simulations [67,68]. The simulation time varied depending on the time serie used (time series are different in relation to duration, from 3 to 7 days) and the data acquisition interval was 900 s because it was used in other studies [34,43]. Lower and upper sides of walls are modelled with a concrete slab. To avoid the influence of thermal bridges produced by the junction with the slab, the internal surface temperature and the heat flux simulated were measured at 1.50 m above the floor. It is worth stressing that monitorings were conducted in different seasons and with different thermal gradients (high and low), with the aim of applying the estimations carried out by the regression models in a wide variety of test conditions. As measurements of the internal surface temperature and the heat flux were available from 163 real tests, they were also used for validating the data simulated. As can be seen in Figure 3, the values simulated were adjusted to the actual values analysed. In these cases, the mean error obtained was 0.23 ºC for the internal surface temperature and 0.14 W/m² for the heat flux. A total of 22,820 different tests were therefore obtained at the end of the simulation process. Figure 4 shows the workflow followed.

Each test was used as an observation of datasets. As 4 different possibilities of approach were distinguished (see Table 1), 4 different datasets were developed. The various input variables considered for each approach were obtained at the end of each test. Given that time series with a different duration were available, the duration of each test was randomly determined, thus implying no coincidences in the time variable among the observations. As the thermophysical properties and thickness of layers must be specified when designing the 140 wall typologies, it is worth stressing that the same accurate knowledge was available to determine U_{6946}.
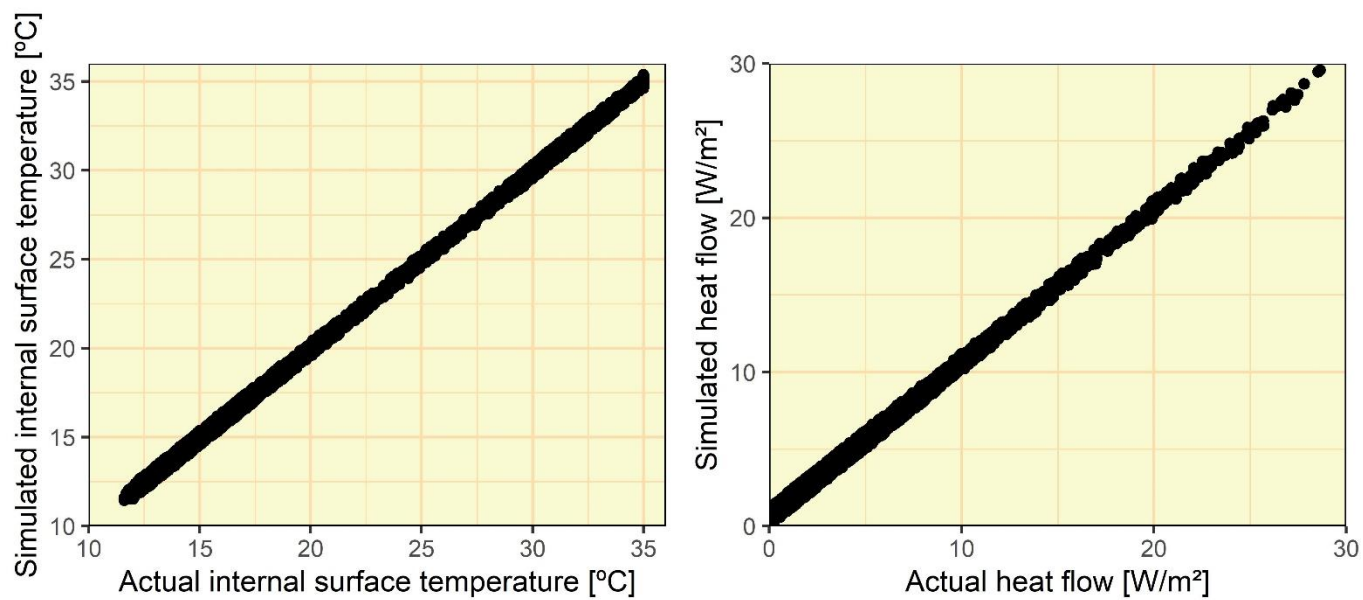
Figure 3. Comparison between the actual and simulated values of the internal surface temperature and the heat flux.
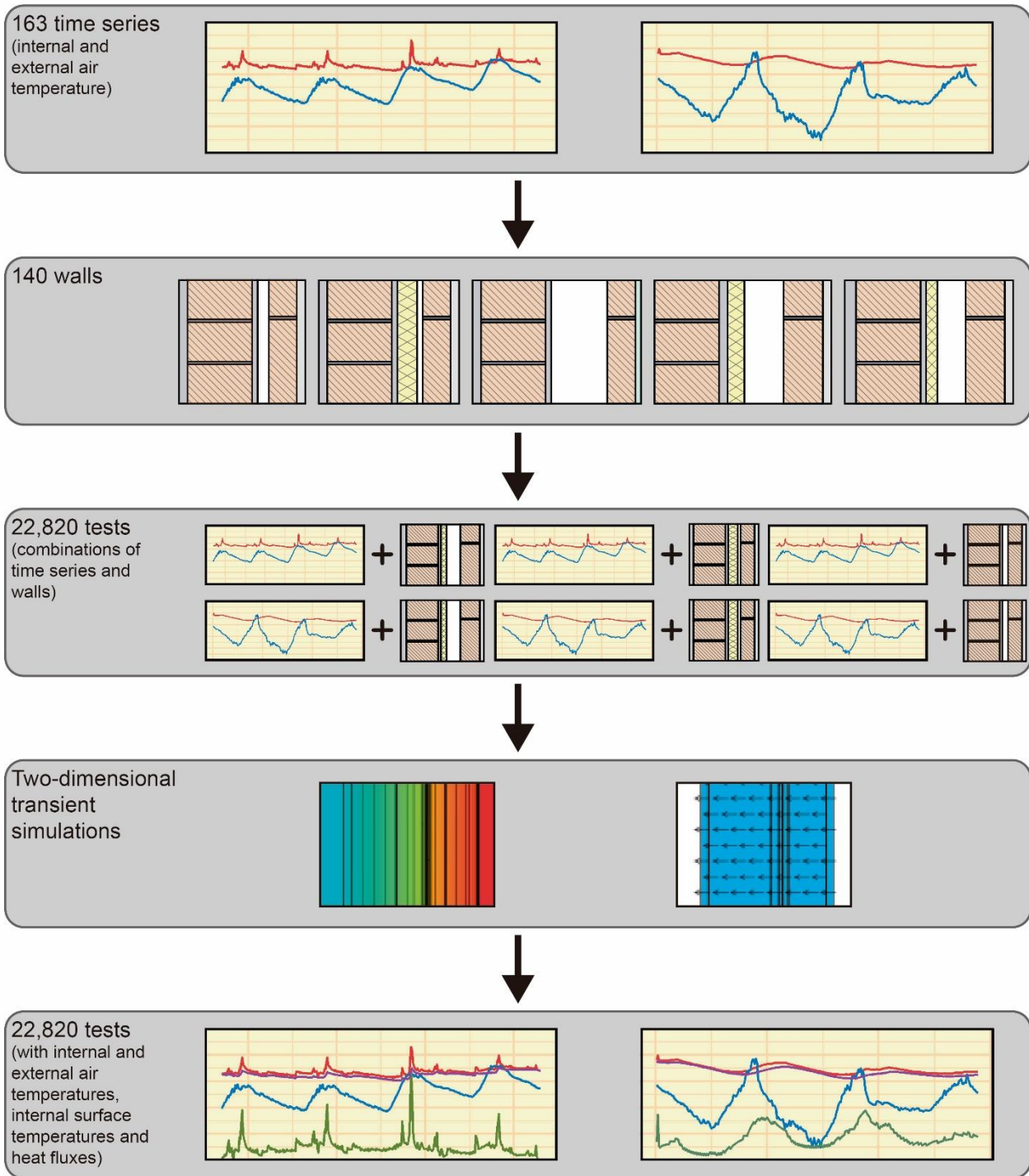
Figure 4. Workflow followed in the simulation process of the 22,820 tests.

4.3. Validation of Random Forest models

A total of 4 different datasets were developed through 22,820 cases simulated. Each dataset was randomly divided into two different subsets: 75% of instances constituted the training subset, and the remaining 25%, the testing subset. The training subset was used in the training phase (i.e., in the developing phase of the model), and the testing subset was used in the testing phase (i.e., in the assessment of the performance of the model with new observations). The training was carried out through a 10-fold cross validation, which reduces the error and the variance of the model [69]. Also, the optimal number of trees used by the model was required to be determined in the training of RF models. For this reason, configurations varying from 1 to 50 trees in each approach were analysed. The most suitable configuration was determined according to the values obtained in the quality statistical parameter. As regression (U_{6946}) and classification (building period) approaches were distinguished in this study, statistical parameters varied. Such indicators were used both in the training and testing. As for regression approaches, the quality indicators were as follows: the coefficient of determination (R^2) (Eq. (9)), the mean absolute error (MAE) (Eq. (10)), and the root mean square error (RMSE) (Eq. (11)). Such parameters have been widely used in many studies to assess the performance of regression models [70,71].

$$R^2 = \left(1 - \frac{\sum_{i=1}^{n}(a_i - e_i)^2}{\sum_{i=1}^{n}(a_i - \bar{a}_i)^2}\right) \tag{9}$$

$$MAE = \frac{\sum_{i=1}^{n}|a_i - e_i|}{n} \tag{10}$$

$$RMSE = \left(\frac{\sum_{i=1}^{n}(a_i - e_i)^2}{n}\right)^{1/2} \tag{11}$$

where a_i is the actual U_{6946}, e_i is the estimated U_{6946}, and n is the number of observations in the dataset.

Regarding the classification approach, the parameters analysed were as follows: the true positive (TP) ratio (Eq. (12)), the false positive (FP) ratio (Eq. (13)), the kappa statistic (Eq. (14)), and the area under the receiver operating characteristic (ROC) curve (Eq. (15)). TP and FP ratios indicate the accuracy percentage in the estimations made by the model, kappa statistic determines the coincidence of the estimation with the real class, and the area under the ROC curve determines the probability that the model classifies correctly the class analysed, existing a different value for each possible label (in this case, there is a value for each building period).

$$TP = \frac{Observations\ correctly\ classified}{Total\ number\ of\ observations} \tag{12}$$

$$FP = \frac{Observations\ incorrectly\ classified}{Total\ number\ of\ observations} \tag{13}$$
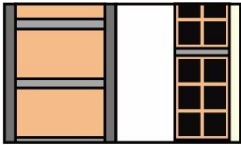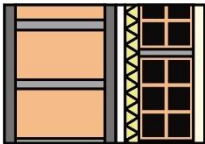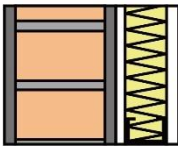
$$K = \frac{p_o - p_e}{1 - p_e} \tag{14}$$

$$AreaROC = \int_0^1 \left(1 - G\big(F^{-1}(1 - t)\big)\right) dt \tag{15}$$

where p_o is the relative observed agreement among the observers, p_e is the hypothetical probability of agreement by chance, and G and F are the distribution of positive and negative samples, respectively.

The performance of the RF models developed with MLPs was also compared to know the advantages of using RF models with respect to a typology of algorithm widely used and validated. In addition, as MLP performs models for classification and regression problems, the results of both approaches could be compared. Datasets were the same as those used for RF models. MLPs were trained by backpropagation [72,73], using the Broyden-Fletcher-Goldfarb-Shanno (BFGS) [74] algorithm. The number of neurons of the hidden layer oscillated between 1 and 20 until determining the optimal architecture by analysing the performance of each architecture with the values obtained in the quality statistical parameters (Eqs. (9)-(15)).

Also, additional monitorings were conducted in 3 actual case studies. Each wall belonged to a building period (see Table 2), thus checking the performance of the models generated with new data from actual monitorings. Measurements were conducted for 1 week and with a data acquisition of 15 min. Surface temperature probes and the heat flux plate were placed in an area without thermal bridges and at a distance of 1.5 m above the floor, following the measurement criterion of variables indicated in Section 4.2 (see Figure 5).

Table 2. Thermophysical properties of the actual walls monitored for being individually analysed.

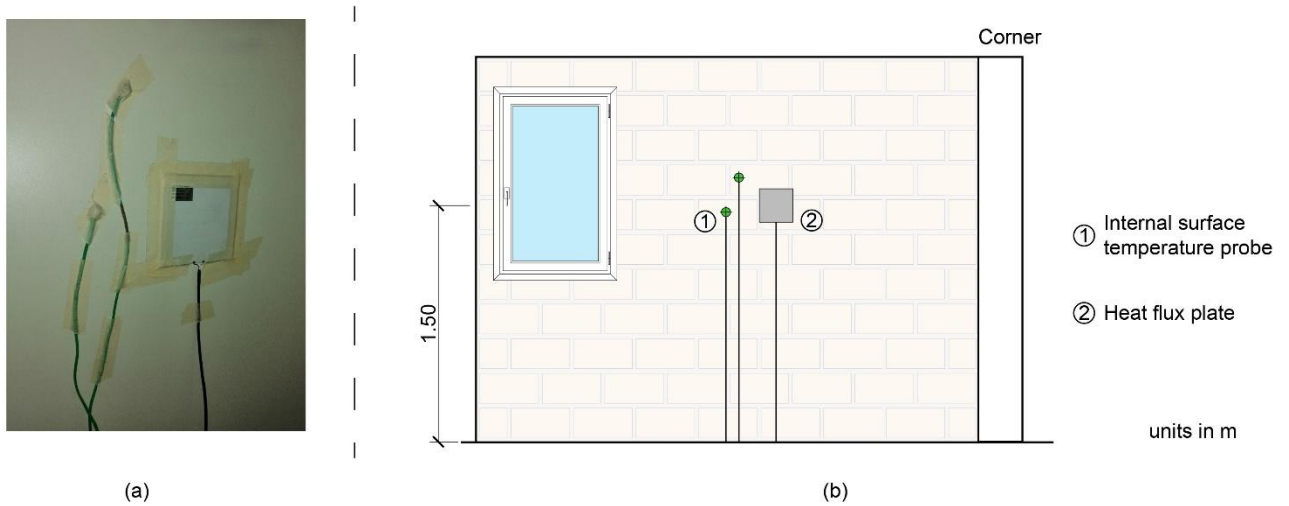| Case	Component	Thickness [m]	Thermal conductivity [W/(mK)]	U-value [W/(m²K)]	Building period	Sketch
Wall A	Cement mortar	0.015	1.000	1.31	P1	
	Solid brick	0.115	0.850			
	Cement mortar	0.015	1.000			
	Air gap	0.100	-			
	Hollow brick	0.070	0.320			
	Gypsum plaster	0.015	0.570			
Wall B	Cement mortar	0.015	1.000	0.69	P2	
	Perforated brick	0.115	0.350			
	Cement mortar	0.015	1.000			
	Air gap	0.010	-			
	MW insulation	0.020	0.038			
	Hollow brick	0.070	0.320			
	Gypsum plaster	0.015	0.570			
Wall C	Cement mortar	0.015	1.000	0.57	P3	
	Perforated brick	0.115	0.350			
	Cement mortar	0.015	1.000			
	Air gap	0.005	-			
	MW insulation	0.040	0.038			
	Laminated plasterboard	0.015	0.250			

Figure 5. Monitoring in actual walls monitored for being individually analysed: (a) photograph of the probes used for monitoring the internal surface temperature and the heat flux, and (b) the placing criterion followed during tests.

5. Results and discussion

5.1. Estimating the U-value of ISO 6946

Firstly, the possibilities of estimating the U-values obtained through ISO 6946 were analysed by using the input variables of both methods. As indicated in Section 3, the determination of the number of trees influenced the performance obtained with Random Forest, so the variability presented by the statistical parameters considered in this study (R^2, MAE, and RMSE) was analysed as the number of trees increased (see Figure 6). Both in the training and testing, the increase of the number of trees led to an improvement of statistical parameters. Regarding HFM models, R^2 was always greater than 99%, with very low values of MAE and RMSE (the highest value of MAE was 0.017, and of RMSE, 0.0635). Also, statistical parameters had acceptable values in THM models. As for the most adequate configuration, the values close to the limit obtained the most acceptable performances. Regarding HFM, it was found that an RF model with 46 trees obtained the best result, whereas in THM, the acceptable result was 42 trees (Table 3). The consideration of a larger number of trees did not imply an improvement of the performance of the models, increasing the computing time and the memory required for the training.

Although the performance obtained by the RF models for HFM and THM was acceptable, a slight deviation was found according to the approach used. Regarding THM models, a slight diminution was obtained in the performance of the model. In this sense, a percentage deviation in R^2 of 0.31% was found in the testing, whereas MAE and RMSE had increases of 82.65% and 78.57%, respectively, so that the modification of input variables meant a variation in the performance of RF models. As mentioned above, the difference between HFM and THM is that the former considers the heat flux, and the latter, the internal surface temperature. The use of heat flux variables leads therefore to a slightly better adjustment in RF models. However, the performance obtained by the RF models of both methods is acceptable: (i) R^2 was greater than 99.55%, and the mean absolute error was lower than 0.0179.
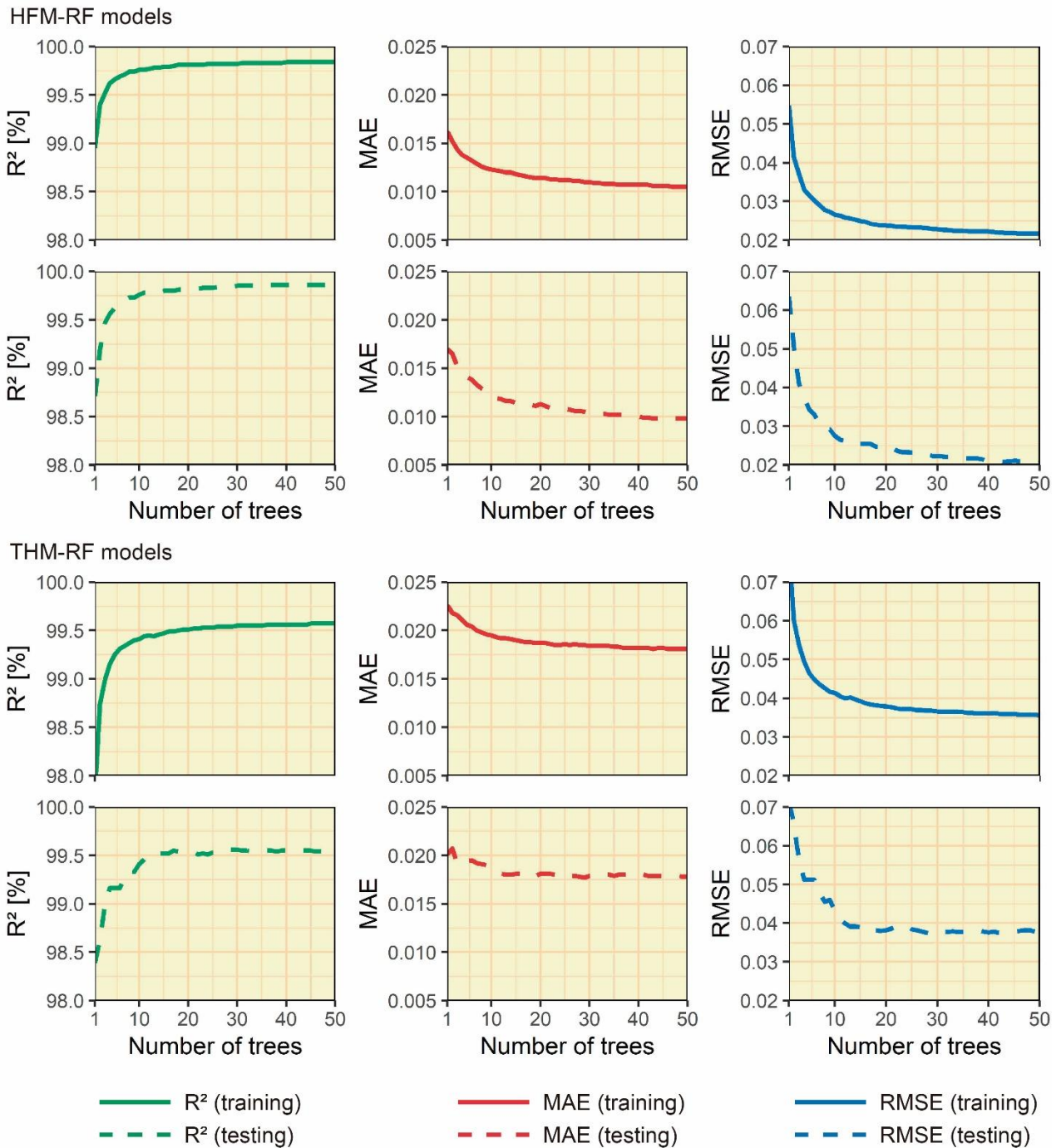
Figure 6. Assessment of the statistical parameters in the training and testing with the variation of the number of trees of RF models to estimate U_{6946}.

Table 3. Performance of the optimal RF models in the testing to estimate U_{6946}.

Method	Model	Number of trees	R^2 [%]	MAE	RMSE
HFM	HFM-RF	46	99.86	0.0098	0.0210
THM	THM-RF	42	99.55	0.0179	0.0375

The performance obtained by the RF models to estimate the U-value included in ISO 6946 was therefore acceptable, thereby leading to accurate estimations. Figures 7 and 8 represent the histograms of the error obtained in the estimations. Moreover, the results of the estimations of the RF models were compared with those obtained by the optimal MLP configurations. The most acceptable architectures of MLPs were of 14 nodes in the hidden layer for HFM, and of 12 nodes in the hidden layer for THM. The error associated with the estimations of the RF models was low. As for the HFM-RF model, 75.14% of estimations had an error between 0 and 0.01 W/(m²K). Such percentage was lower in the case of the MLP, with 21.27% of estimations with error values in such range. Also, the error values were greater in HFM-MLP: whereas the error values ranged from -0.181 to 0.167 W/(m²K) in HFM-RF, the values ranged from -0.318 to 0.324 W/(m²K) in HFM-MLP. Although HFM-RF obtained slightly high error values, the number of observations was low. In this sense, the percentage of instances with errors greater than 0.05 W/(m²K) was 3%, whereas in the case of HFM-MLP, the percentage was 26.82%.
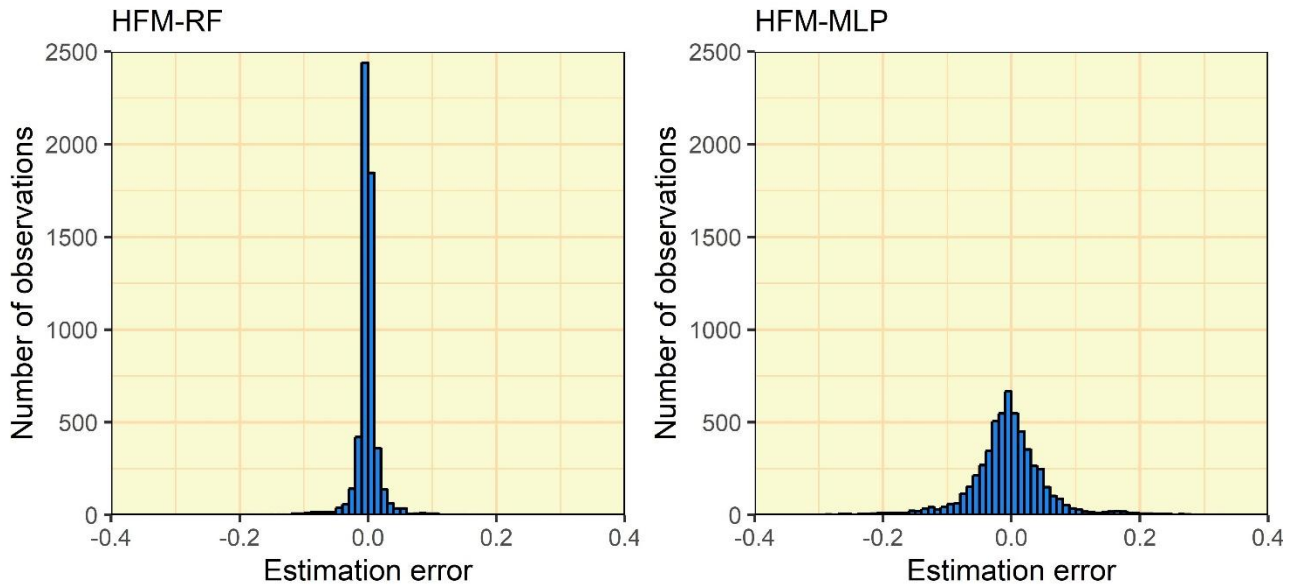
Figure 7. Comparison of the errors between the values estimated by the HFM models and the actual values in the testing phase. The histogram is represented by a bin width of 0.01 W/(m²K).

THM models had similar tendencies as HFM models. The THM-RF model made estimations with an acceptable accuracy degree. The percentage of observations with a range of error between 0 and 0.01 W/(m²K) was 57.18% in RF, whereas it was 14.44% in MLP. Likewise, the range of errors was smaller in THM-RF than in THM-MLP, although the difference between the limit values was reduced: the error values of THM-RF ranged from -0.295 to 0.265 W/(m²K), and the error values of THM-MLP were between -0.311 and 0.397. This same tendency was found in the percentage of instances in such ranges: 7.52% in THM-RF and 35.71% in THM-MLP.
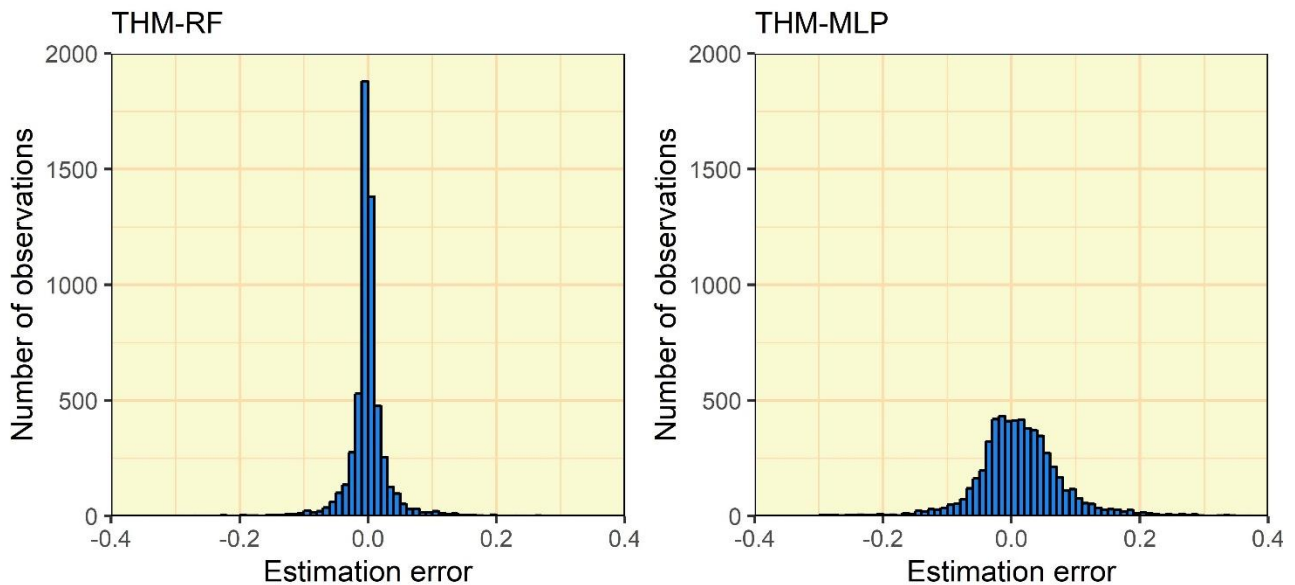

Figure 8. Comparison of the errors between the values estimated by the THM models and the actual values in the testing phase. The histogram is represented by a bin width of 0.01 W/(m²K).

The use of RF models therefore obtained adjusted estimations of the thermal transmittance of ISO 6946, both in HFM and THM. Although some differences in the performance of RF models were found according to the type of input variables (i.e., the in-situ assessment method), the estimation made by the models had deviations lower than 0.05 W/(m²K) in more than 92.48% of the tests analysed (97% in HFM-RF and 92.48% in THM-RF). This tendency was found in the analysis of the estimations conducted in the walls for being individually analysed (see Table 4). In these cases, the estimations conducted by the RF models were adjusted (with an error lower than 0.01 W/(m²K)), whereas in the MLP models, errors between 0.01 and 0.09 W/(m²K) were achieved. RF models can therefore be used as a methodology to validate the experimental results obtained by HFM and THM.

Table 4. Results of the estimations of U_{6946} conducted by the models in the walls individually analysed.

Wall	U_{6946} [W/(m²K)]	Estimated U-value [W/(m²K)]			
		HFM-RF	THM-RF	HFM-MLP	THM-MLP
Wall A	1.31	1.30	1.31	1.38	1.35
Wall B	0.69	0.69	0.69	0.66	0.67
Wall C	0.57	0.56	0.57	0.66	0.61

5.2. Estimating the building period for heat storage corrections

After validating the use of RF models to determine accurately the thermal transmittance obtained through ISO 6946, their performance was analysed in the estimation of the building period. As in Section 5.1, the most adequate number of trees for RF models was determined (see Figure 9). Both in HFM-RF and THM-RF, the increase of the number of trees from 1 to 30 had an increase in the performance of the models. Over 30, the most acceptable configurations were determined for each approach: for HFM-RF, the optimal number was 33 trees, and for THM-RF, 30. Over such numbers, the performance of the models did not improve, leading to an increase of the computing time.
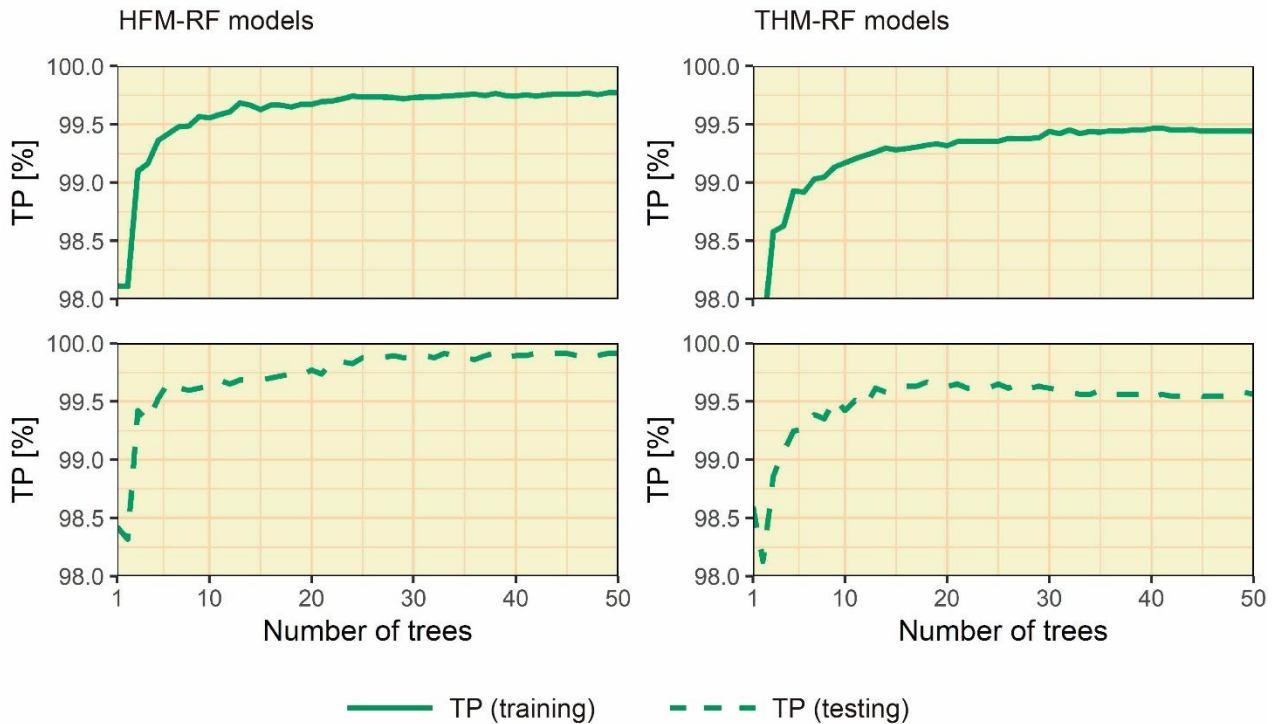

Figure 9. Evaluation of the TP ratio in the training and testing with the variation of the number of trees of the RF models.

After determining the most acceptable configuration for each methodology, the results were compared with the optimal MLPs. The analysis determined that MLP configurations with 13 and 15 nodes in the hidden layer were the best for HFM and THM, respectively. Figure 10 shows the performances obtained by the HFM models in the testing. Firstly, the analysis of the confusion matrix of HFM-RF showed the high TP ratio in the 3 building periods (in the confusion matrix, diagonal values correspond to the TP ratio, whereas the other values are the FP ratio). In this sense, the TP ratio in P1 was 100%, whereas in P2 and P3 was 99.72 and 99.92%, respectively. The classification was therefore optimal in most observations. However, a certain limitation was found in some instances of P2 and P3 because such building periods had certain similarities (e.g., the use of insulation), unlike P1. Such TP ratios were different from that obtained in HFM-MLP. This model showed how the building periods of the walls were worse classified. So, the TP ratio in P1 was 95.41%; in P2, 87.36%, and in P3, 99.16%. The model was found to present the high FP ratio in the next building period in which it should be classified (e.g., the high FP ratio was presented in P2 when it should be classified in P1), thus showing the limitations of MLP to determine the differences among building periods.

On the other hand, the kappa statistic and the area under the ROC curve had very different values between the models. The area under the ROC curve determines the probability that the model correctly classifies the class analysed, whereas the kappa statistic determines the coincidence of the class estimated with the real class. Values close to 1 of both parameters indicates a better estimation of the models. HFM-RF and HFM-MLP obtained values close to 1 in both parameters. However, HFM-RF obtained better values than HFM-MLP: (i) the kappa statistic obtained a value very close to 1 in HFM-RF, whereas its value was 0.914 in HFM-MLP; and (ii) the area under the ROC curve of the three building periods was 1 in HFM-RF, whereas lower values were obtained in HFM-MLP (0.993 for P1, 0.972 for P2, and 0.988 for P3). Such differences showed the worse performance presented by HFM-MLP to correctly estimate the building periods of the observations of the testing dataset.

Regarding the models developed for THM, a similar behaviour was found when building periods were to be classified (see Figure 11). THM-RF had a greater TP ratio than THM-MLP. Also, both the statistic kappa and the area under the ROC curve were better in THM-RF than in THM-MLP. Regarding walls for their individual analysis, a behaviour similar to what is above indicated was found, conducting correct estimations of the building period with all models except THM-MLP (see Table 5).

Table 5. Results of the estimations of the building period conducted by the models in the walls individually analysed.

Wall	Period	Estimated period			
		HFM-RF	THM-RF	HFM-MLP	THM-MLP
Wall A	P1	P1	P1	P1	P1
Wall B	P2	P2	P2	P2	P2
Wall C	P3	P3	P3	P3	P2

HFM-RF model

	P1 (pred.)	P2 (pred.)	P3 (pred.)
P1 (actual)	100.00 %	0.00 %	0.00 %
P2 (actual)	0.06 %	99.72 %	0.22 %
P3 (actual)	0.00 %	0.08 %	99.92 %

HFM-MLP model

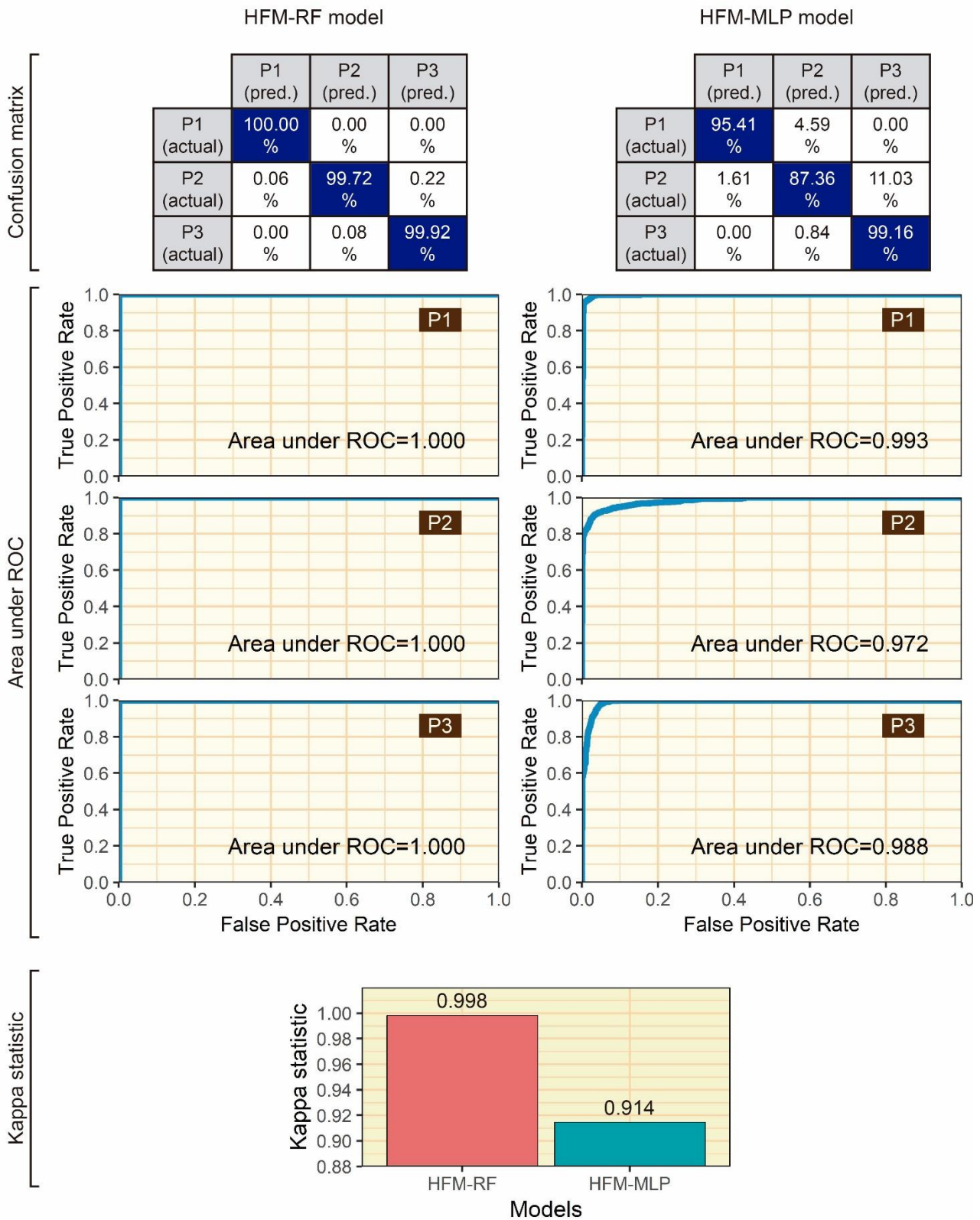|	P1 (pred.)	P2 (pred.)	P3 (pred.)
P1 (actual)	95.41 %	4.59 %	0.00 %
P2 (actual)	1.61 %	87.36 %	11.03 %
P3 (actual)	0.00 %	0.84 %	99.16 %

Figure 10. Comparison of the performance obtained between HFM-RF and HFM-MLP models in the estimation of the building periods of the wall.
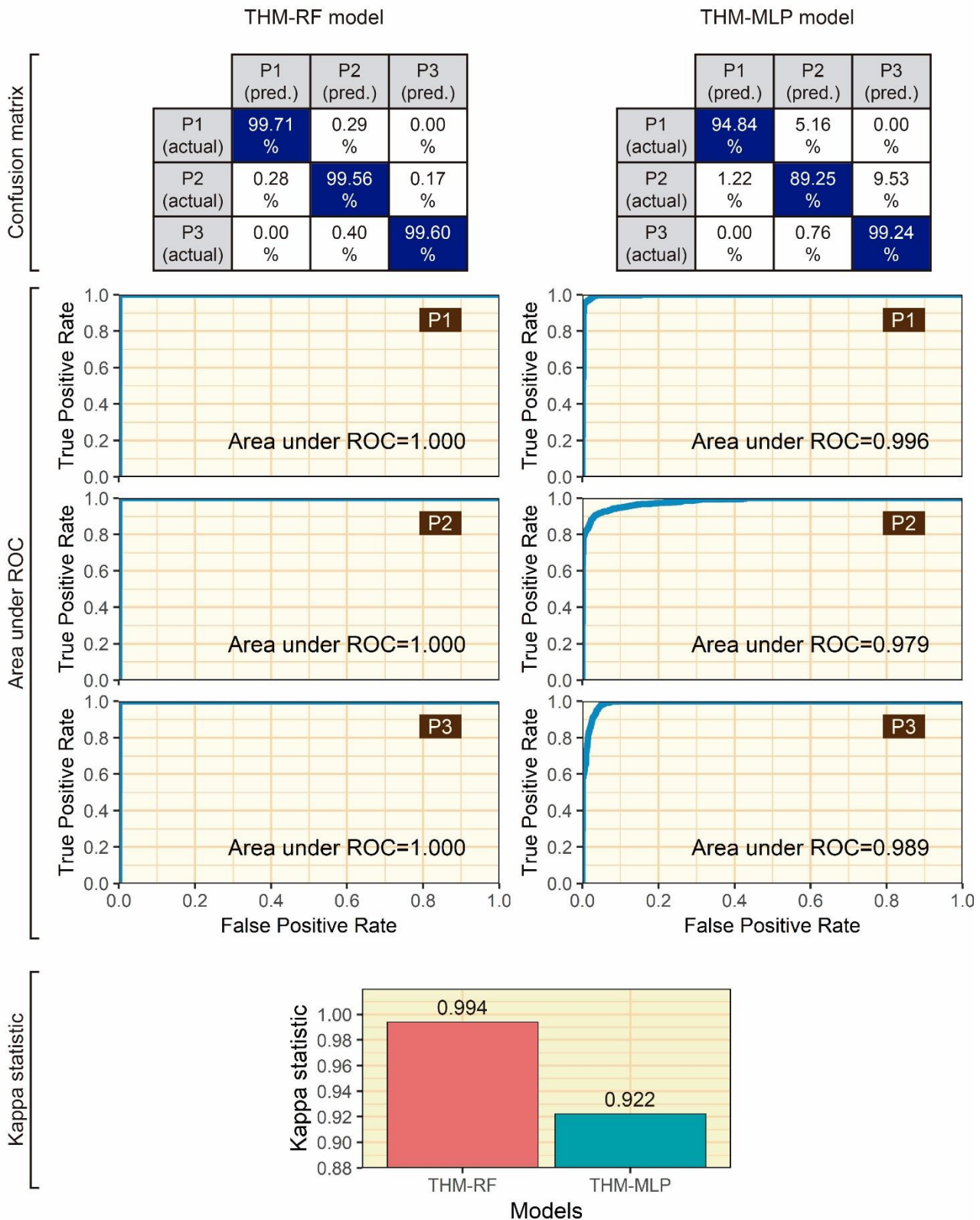
Figure 11. Comparison of the performance obtained between THM-RF and THM-MLP models in the estimation of the building periods of the wall.

The results therefore showed how the models developed with the RF algorithm classified correctly the building periods of the simulated tests. Also, its performance was better than the MLPs developed with the same dataset. Although MLPs have a potential of use for various assessment applications of the thermal transmittance, as those developed by Bienvenido-Huertas et al. [43] and Buratti et al. [75], their use is limited to determine the thermal transmittance included in ISO 6946 and the building period of walls with monitored data. The limitations are solved by the models developed with the RF algorithm. In addition, the results of this study stress the potential of using algorithms of artificial intelligence different from MLPs to tackle the problems related to the thermal characterization of buildings.

6. Conclusions

This study analyses the optimization and automation of certain processes related to the assessment of the thermal transmittance of walls. Particularly, two aspects were analysed according to the limitations showed in the scientific literature: (i) the determination of the thermal transmittance of ISO 6946 to validate the experimental results following section 7.3 from ISO 9869-1; and (ii) the determination of the building period of walls to apply the optimized procedure of correction for storage effects developed in a previous study [43]. Random Forest models were designed for the two most used assessment methodology of thermal transmittance: the heat flow meter method and the thermometric method.

Based on the results obtained, Random Forest models had an efficient performance for the applications proposed. On the one hand, as for the determination of the thermal transmittance of ISO 6946, models made estimations with a correlation coefficient greater than 99.55% with respect to the real values. On the other hand, more than 5,276 of the 5,705 tests analysed in the testing had errors lower than 0.05 $W/(m^2K)$ in the estimation. Also, by comparing the Random Forest models with multilayer perceptrons, it was found that the former is the most adequate typology of algorithm to determine the thermal transmittance of ISO 6946.

This same tendency was found in the approach to determine the building period of walls. In this approach, the true positive ratio in the 3 periods was always greater than 99.50% in the various Random Forest models, whereas a greater error in the true positive ratio was obtained in the multilayer perceptrons.

Results firstly showed the suitability of using the Random Forest algorithm to determine the thermal transmittance and the building period of a wall by its monitoring (whether by the heat flow meter method or the thermometric method), and secondly, the potential of using other algorithms of artificial intelligence different from the multilayer perceptrons, thus optimizing and automating certain processes related to the building thermal characterization.

To conclude, the relevance of this study is the proposal of two new applications allowing the uncertainty associated with the problems analysed to be reduced. On the one hand, many studies reveal the limitations when determining the thermal transmittance of ISO 6946 because of the uncertainty associated with the determination of layers, material, and thermophysical properties of walls. Such determination, however, is essential to have a reference value to determine whether the results obtained by any in-situ procedure (e.g., the heat flow meter method) are representative. On the other hand, knowing the representative building period of the zone in which a wall was built is required by the correction for storage effect designed in a previous study. Although consulting cadastral data could solve this aspect, there can always be some uncertainty whether the wall was designed according to the technical regulation of that period. The results of this study therefore remove the error sources associated with thermal characterization tests and could be useful for energy auditors, architects, and engineers. Also, the methodology used to generate datasets to train and validate the models (based on the combination of real data and simulations) would adapt models to the building periods which are typical of each zone. Finally, a more automatized process to characterize the thermal transmittance would establish better energy conservation measures, reduce payback periods, and ensure a greater renovation rate of the building stock, thus facilitating the objective proposed by the European Union by 2050: reducing the greenhouse gas emissions of building sector by 90%.

References

[1]   Intergovernmental Panel on Climate Change, Climate change 2014: synthesis report. Contribution of working groups I, II and III to the fifth assessment report of the intergovernmental Panel on climate change, Cambridge University Press, Cambridge, 2014. doi:10.1017/CBO9781107415324.004.

[2]   European Commission, A Roadmap for moving to a competitive low carbon economy in 2050, Brussels, Belgium, 2011.

[3]   N.A. Kurekci, Determination of optimum insulation thickness for building walls by using heating and cooling degree-day values of all Turkey's provincial centers, Energy Build. 118 (2016) 197–213. doi:10.1016/j.enbuild.2016.03.004.

[4]   V. Echarri-Iribarren, C. Rizo-Maestre, J.L. Sanjuan-Palermo, Underfloor heating using ceramic thermal panels and solar thermal panels in public buildings in the Mediterranean: Energy savings and healthy indoor environment, Appl. Sci. 9 (2019) 1–18. doi:10.3390/app9102089.

[5]   M. Teni, K. Čulo, H. Krstić, Renovation of Public Buildings towards nZEB: A Case Study of a Nursing Home, Buildings. 9 (2019) 153. doi:10.3390/buildings9070153.

[6]   V. Echarri-Iribarren, C. Sotos-Solano, A. Espinosa-Fernández, R. Prado-Govea, The Passivhaus standard in the Spanish Mediterranean: Evaluation of a house's thermal behaviour of enclosures and airtightness, Sustain. 11 (2019). doi:10.3390/su11133732.

[7]   D. Bienvenido-Huertas, J. Moyano, D. Marín, R. Fresco-Contreras, Review of in situ methods for assessing the thermal transmittance of walls, Renew. Sustain. Energy Rev. 102 (2019) 356–371. doi:10.1016/j.rser.2018.12.016.

[8]   International Organization for Standardization, ISO 9869-1:2014 - Thermal insulation - Building elements - In situ measurement of thermal resistance and thermal transmittance. Part 1: Heat flow meter method, Geneva, Switzerland, 2014.

[9]   P.G. Cesaratto, M. De Carli, S. Marinetti, Effect of different parameters on the in situ thermal conductance evaluation, Energy Build. 43 (2011) 1792–1801. doi:10.1016/j.enbuild.2011.03.021.

[10] G. Desogus, S. Mura, R. Ricciu, Comparing different approaches to in situ measurement of building components thermal resistance, Energy Build. 43 (2011) 2613–2620. doi:10.1016/j.enbuild.2011.05.025.

[11] H. Trethowen, Measurement errors with surface-mounted heat flux sensors, Build. Environ. 21 (1986) 41–56. doi:10.1016/0360-1323(86)90007-7.

[12] X. Meng, B. Yan, Y. Gao, J. Wang, W. Zhang, E. Long, Factors affecting the in situ measurement accuracy of the wall heat transfer coefficient using the heat flow meter method, Energy Build. 86 (2015) 754–765. doi:10.1016/j.enbuild.2014.11.005.

[13] K. Gaspar, M. Casals, M. Gangolells, Energy & Buildings In situ measurement of façades with a low U-value : Avoiding deviations, Energy Build. 170 (2018) 61–73. doi:10.1016/j.enbuild.2018.04.012.

[14] A. Ahmad, M. Maslehuddin, L.M. Al-Hadhrami, In situ measurement of thermal transmittance and thermal resistance of hollow reinforced precast concrete walls, Energy Build. 84 (2014) 132–141. doi:10.1016/j.enbuild.2014.07.048.

[15] G. Litti, S. Khoshdel, A. Audenaert, J. Braet, Hygrothermal performance evaluation of traditional brick masonry in historic buildings, Energy Build. 105 (2015) 393–411. doi:10.1016/j.enbuild.2015.07.049.

[16] I.N. Grubeša, M. Teni, H. Krstić, M. Vračević, Influence of freeze/thaw cycles on mechanical and thermal properties of masonry wall and masonry wall materials, Energies. 12 (2019) 1–11. doi:10.3390/en12081464.

[17] K. Gaspar, M. Casals, M. Gangolells, Review of criteria for determining HFM minimum test duration, Energy Build. 176 (2018) 360–370. doi:10.1016/j.enbuild.2018.07.049.

[18] D.S. Choi, M.J. Ko, Analysis of convergence characteristics of average method regulated by iso 9869-1 for evaluating in situ thermal resistance and thermal transmittance of opaque exterior walls, Energies. 12 (2019) 1–18. doi:10.3390/en12101989.

[19] G. Ficco, F. Iannetta, E. Ianniello, F.R. D'Ambrosio Alfano, M. Dell'Isola, U-value in situ measurement for energy diagnosis of existing buildings, Energy Build. 104 (2015) 108–121. doi:10.1016/j.enbuild.2015.06.071.

[20] L. Evangelisti, C. Guattari, P. Gori, F. Bianchi, Heat transfer study of external convective and radiative coefficients for building applications, Energy Build. 151 (2017) 429–438. doi:10.1016/j.enbuild.2017.07.004.

[21] F. Asdrubali, F. D'Alessandro, G. Baldinelli, F. Bianchi, Evaluating in situ thermal transmittance of green buildings masonries: A case study, Case Stud. Constr. Mater. 1 (2014) 53–59. doi:10.1016/j.cscm.2014.04.004.

[22] E. Lucchi, Thermal transmittance of historical brick masonries: A comparison among standard data, analytical calculation procedures, and in situ heat flow meter measurements, Energy Build. 134 (2017) 171–184. doi:10.1016/j.enbuild.2016.10.045.

[23] E. Lucchi, Thermal transmittance of historical stone masonries: A comparison among standard, calculated and measured data, Energy Build. 151 (2017) 393–405. doi:10.1016/j.enbuild.2017.07.002.

[24] M. Rotilio, F. Cucchiella, P. De Berardinis, V. Stornelli, Thermal Transmittance Measurements of the Historical Masonries: Some Case Studies, Energies. 11 (2018) 2987. doi:10.3390/en11112987.

[25] I. Nardi, E. Lucchi, T. de Rubeis, D. Ambrosini, Quantification of heat energy losses through the building envelope: A state-of-the-art analysis with critical and comprehensive review on infrared thermography, Build. Environ. 146 (2018) 190–205. doi:10.1016/j.buildenv.2018.09.050.

[26] R. Albatici, A.M. Tonelli, Infrared thermovision technique for the assessment of thermal transmittance value of opaque building elements on site, Energy Build. 42 (2010) 2177–2183. doi:10.1016/j.enbuild.2010.07.010.

[27] G. Dall'O', L. Sarto, A. Panza, Infrared screening of residential buildings for energy audit purposes: Results of a field test, Energies. 6 (2013) 3859–3878. doi:10.3390/en6083859.

[28] P.A. Fokaides, S.A. Kalogirou, Application of infrared thermography for the determination of the overall heat transfer coefficient (U-Value) in building envelopes, Appl. Energy. 88 (2011) 4358–4365. doi:10.1016/j.apenergy.2011.05.014.

[29] R. Madding, Finding R-Values of Stud Frame Constructed Houses with IR Thermography, Proc. InfraMation. (2008).

[30] B. Tejedor, M. Casals, M. Gangolells, X. Roca, Quantitative internal infrared thermography for determining in-situ thermal behaviour of façades, Energy Build. 151 (2017) 187–197. doi:10.1016/j.enbuild.2017.06.040.

[31] D. Bienvenido-Huertas, J. Bermúdez, J. Moyano, D. Marín, Comparison of quantitative IRT to estimate U-value using different approximations of ECHTC in multi-leaf walls, Energy Build. 184 (2019) 99–113. doi:10.1016/j.enbuild.2018.11.028.

[32] D. Bienvenido-Huertas, J. Bermúdez, J.J. Moyano, D. Marín, Influence of ICHTC correlations on the thermal characterization of façades using the quantitative internal infrared thermography method, Build. Environ. 149 (2019) 512–525. doi:10.1016/j.buildenv.2018.12.056.

[33] B. Tejedor, M. Casals, M. Gangolells, Assessing the influence of operating conditions and thermophysical properties on the accuracy of in-situ measured U-values using quantitative internal infrared thermography, Energy Build. 171 (2018) 64–75. doi:10.1016/j.enbuild.2018.04.011.

[34] D. Bienvenido-Huertas, R. Rodríguez-Álvaro, J.J. Moyano, F. Rico, D. Marín, Determining the U-Value of Façades Using the Thermometric Method: Potentials and Limitations, Energies. 11 (2018) 1–17. doi:10.3390/en11020360.

[35] S.-H. Kim, J.-H. Lee, J.-H. Kim, S.-H. Yoo, H.-G. Jeong, The Feasibility of Improving the Accuracy of In Situ Measurements in the Air-Surface Temperature Ratio Method, Energies. 11 (2018) 1–18. doi:10.3390/en11071885.

[36] S.-H. Kim, J.-H. Kim, H.-G. Jeong, K.-D. Song, Reliability Field Test of the Air–Surface Temperature Ratio Method for In Situ Measurement of U-Values, Energies. 11 (2018) 1–15. doi:10.3390/en11040803.

[37] International Organization for Standardization, ISO 6946:2007 - Building components and building elements - Thermal resistance and thermal transmittance - Calculation method, Geneva, Switzerland, 2007.

[38] K. Gaspar, M. Casals, M. Gangolells, A comparison of standardized calculation methods for in situ measurements of

façades U-value, Energy Build. 130 (2016) 592–599. doi:10.1016/j.enbuild.2016.08.072.

[39] V. Echarri, A. Espinosa, C. Rizo, Thermal transmission through existing building enclosures: Destructive monitoring in intermediate layers versus non-destructive monitoring with sensors on surfaces, Sensors. 17 (2017) 1–24. doi:10.3390/s17122848.

[40] I. Ballarini, S.P. Corgnati, V. Corrado, Use of reference buildings to assess the energy saving potentials of the residential building stock: The experience of TABULA project, Energy Policy. 68 (2014) 273–284. doi:10.1016/j.enpol.2014.01.027.

[41] D.S. Choi, M.J. Ko, Comparison of Various Analysis Methods Based on Heat Flowmeters and Infrared Thermography Measurements for the Evaluation of the In Situ Thermal Transmittance of Opaque Exterior Walls, Energies. 10 (2017) 1–22. doi:10.3390/en10071019.

[42] A.H. Deconinck, S. Roels, Comparison of characterisation methods determining the thermal resistance of building components from onsite measurements, Energy Build. 130 (2016) 309–320. doi:10.1016/j.enbuild.2016.08.061.

[43] D. Bienvenido-Huertas, J. Moyano, C.E. Rodríguez-Jiménez, D. Marín, Applying an artificial neural network to assess thermal transmittance in walls by means of the thermometric method, Appl. Energy. 233–234 (2019) 1–14. doi:10.1016/j.apenergy.2018.10.052.

[44] D. Bienvenido-Huertas, C. Rubio-Bellido, J.L. Pérez-Ordóñez, J. Moyano, Optimizing the evaluation of thermal transmittance with the thermometric method using multilayer perceptrons, Energy Build. 198 (2019) 395–411. doi:10.1016/j.enbuild.2019.06.040.

[45] L. Evangelisti, C. Guattari, P. Gori, R. de Lieto Vollaro, F. Asdrubali, Experimental investigation of the influence of convective and radiative heat transfers on thermal transmittance measurements, Int. Commun. Heat Mass Transf. 78 (2016) 214–223. doi:10.1016/j.icheatmasstransfer.2016.09.008.

[46] E. Sassine, Y. Cherif, E. Antczak, Parametric identification of thermophysical properties in masonry walls of buildings, J. Build. Eng. 25 (2019) 100801. doi:10.1016/j.jobe.2019.100801.

[47] P. Santos, M. Gonçalves, C. Martins, N. Soares, J.J. Costa, Thermal transmittance of lightweight steel framed walls: Experimental versus numerical and analytical approaches, J. Build. Eng. 25 (2019) 100776. doi:10.1016/j.jobe.2019.100776.

[48] D. Chong, N. Zhu, W. Luo, X. Pan, Human thermal risk prediction in indoor hyperthermal environments based on random forest, Sustain. Cities Soc. 49 (2019) 101595. doi:10.1016/j.scs.2019.101595.

[49] T. Chaudhuri, D. Zhai, Y.C. Soh, H. Li, L. Xie, Random forest based thermal comfort prediction from gender-specific physiological parameters using wearable sensing technology, Energy Build. 166 (2018) 391–406. doi:10.1016/j.enbuild.2018.02.035.

[50] L. Benali, G. Notton, A. Fouilloy, C. Voyant, R. Dizene, Solar radiation forecasting using artificial neural network and random forest methods: Application to normal beam, horizontal diffuse and global components, Renew. Energy. 132 (2019) 871–884. doi:10.1016/j.renene.2018.08.044.

[51] L. Breiman, J. Friedman, C.J. Stone, R.A. Olshen, Classification and regression trees, Routledge, 2017.

[52] G.K.F. Tso, K.K.W. Yau, Predicting electricity energy consumption: A comparison of regression analysis, decision tree and neural networks, Energy. 32 (2007) 1761–1768. doi:10.1016/j.energy.2006.11.010.

[53] W.A.Y. Mousa, W. Lang, T. Auer, W.A. Yousef, A pattern recognition approach for modeling the air change rates in naturally ventilated buildings from limited steady-state CFD simulations, Energy Build. 155 (2017) 54–65. doi:10.1016/j.enbuild.2017.09.016.

[54] S. Dudoit, J. Fridlyand, T.P. Speed, Comparison of discrimination methods for the classification of tumors using gene expression data, J. Am. Stat. Assoc. 97 (2002) 77–87.

[55] B. Larivière, D. Van Den Poel, Predicting customer retention and profitability by using random forests and regression forests techniques, Expert Syst. Appl. 29 (2005) 472–484. doi:10.1016/j.eswa.2005.04.043.

[56] T.G. Dietterich, Experimental comparison of three methods for constructing ensembles of decision trees: bagging, boosting, and randomization, Mach. Learn. 40 (2000) 139–157. doi:10.1023/A:1007607513941.

[57] L. Breiman, Bagging predictors, Mach. Learn. 24 (1996) 123–140.

[58] L. Breiman, Random forests, Mach. Learn. 45 (2001) 5–32. doi:10.1023/A:1010933404324.

[59] D. Assouline, N. Mohajeri, J.L. Scartezzini, Large-scale rooftop solar photovoltaic technical potential estimation using Random Forests, Appl. Energy. 217 (2018) 189–211. doi:10.1016/j.apenergy.2018.02.118.

[60] Y. Zhou, G. Qiu, Random forest for label ranking, Expert Syst. Appl. 112 (2018) 99–109. doi:10.1016/j.eswa.2018.06.036.

[61] V. Rodriguez-Galiano, M. Sanchez-Castillo, M. Chica-Olmo, M. Chica-Rivas, Machine learning predictive models for mineral prospectivity: An evaluation of neural networks, random forest, regression trees and support vector machines, Ore Geol. Rev. 71 (2015) 804–818. doi:10.1016/j.oregeorev.2015.01.001.

[62] The Government of Spain, Royal Decree 2429/79. Approving the Basic Building Norm NBE-CT-79, about the Thermal Conditions in Buildings, 1979.

[63] The Government of Spain, Royal Decree 314/2006. Approving the Spanish Technical Building Code, Madrid, Spain, 2013.

[64] Eduardo Torroja Institute for Construction Science, Constructive elements catalogue of the CTE, 2010.

[65] F. Kurtz, M. Monzón, B. López-Mesa, Energy and acoustics related obsolescence of social housing of Spain's post-war in less favoured urban areas. The case of Zaragoza, Inf. La Construcción. 67 (2015) m021. doi:10.3989/ic.14.062.

[66] S. Domínguez-Amarillo, J.J. Sendra, I. Oteiza, La envolvente térmica de la vivienda social. El caso de Sevilla, 1939 a 1979, Editorial CSIC: Madrid, 2016.

[67]   L. Evangelisti, C. Guattari, F. Asdrubali, Influence of heating systems on thermal transmittance evaluations: Simulations, experimental measurements and data post-processing, Energy Build. 168 (2018) 180–190. doi:10.1016/j.enbuild.2018.03.032.

[68]   D. Bienvenido-Huertas, C. Rubio-Bellido, D. Sánchez-García, J. Moyano, Internal surface condensation risk in façades of Spanish social dwellings, Build. Res. Inf. 0 (2019) 1–20. doi:10.1080/09613218.2019.1612729.

[69]   R. Kohavi, A Study of Cross-Validation and Bootstrap for Accuracy Estimation and Model Selection, in: Int. Jt. Conf. Artif. Intell., 1995. doi:10.1067/mod.2000.109031.

[70]   D. Bienvenido-Huertas, A. Pérez-Fargallo, R. Alvarado-Amador, C. Rubio-Bellido, Influence of climate on the creation of multilayer perceptrons to analyse the risk of fuel poverty, Energy Build. 198 (2019) 38–60. doi:10.1016/j.enbuild.2019.05.063.

[71]   R. Pino-Mejías, A. Pérez-Fargallo, C. Rubio-Bellido, J.A. Pulido-Arcas, Comparison of linear regression and artificial neural networks models to predict heating and cooling energy demand, energy consumption and CO2 emissions, Energy. 118 (2017) 24–36. doi:10.1016/j.energy.2016.12.022.

[72]   D.E. Rumelhart, G.E. Hinton, R.J. Williams, Learning representations by back-propagating errors, Nature. 323 (1986) 533–536. doi:10.1038/323533a0.

[73]   Y.N. Wang, A neural network adaptive control based on rapid learning method and application, Adv. Molding Anal. 46 (1994) 27–34.

[74]   R. Fletcher, Practical methods of optimization, John Wiley&Sons, Chichester - New York - Brisbane - Toronto, United States, 1980.

[75]   C. Buratti, L. Barelli, E. Moretti, Application of artificial neural network to predict thermal transmittance of wooden windows, Appl. Energy. 98 (2012) 425–432. doi:10.1016/j.apenergy.2012.04.004.